Journal of Geophysical Research – Atmospheres

Supporting Information for

Investigating drivers of particulate matter pollution over India and the implications for radiative forcing with GEOS-Chem-TOMAS15

Authors: Alexandra Karambelas[1,*], Arlene M. Fiore[1,2,^], Daniel M. Westervelt[1,7], V. Faye McNeill[3], Cynthia A. Randles[4], Chandra Venkataraman[5], Jeffrey R. Pierce[6], Kelsey R. Bilsback[6], George P. Milly[1]

[1] Lamont-Doherty Earth Observatory, Columbia University, Palisades, NY USA
* Now at Northeast States for Coordinated Air Use Management, Boston, MA USA
[2] Department of Earth and Environmental Sciences, Columbia University, New York, NY USA
^Now at Department of Earth, Atmospheric and Planetary Sciences, Massachusetts Institute of Technology, Cambridge, MA, USA
[3] Chemical and Environmental Engineering, Columbia University, New York, NY USA
[4] ExxonMobil Technology and Engineering Company, Annandale, NJ USA
[5] Department of Chemical Engineering, Indian Institute of Technology Bombay, Mumbai, India
[6] Department of Atmospheric Science, Colorado State University, Fort Collins, CO USA
[7] NASA Goddard Institute for Space Studies, New York, NY, USA

Contents of this file

Detailed information on GEOS-Chem

We use GEOS-Chem v12.0.2 for all global and nested India simulations. Emissions mostly follow standard GEOS-Chem simulations that use HEMCO (Keller et al., 2014). A summary is included below, but more details on the emissions and HEMCO including additional references are available at http://wiki.seas.harvard.edu/geos-chem/index.php/The_HEMCO_User%27s_Guide#References.

Anthropogenic emissions for GC-Tropchem and GC-TOMAS15 simulation include ECLIPSE v5a global emissions inventory. We apply the following emissions overlays in the global simulation: hourly NEI 2011 emissions for the U.S., BRAVO emissions for Mexico, APEI emissions for Canada, EMEP emissions for Europe, and DICE emissions for Africa (Marais and Wiedinmyer, 2016). Supplemental inventories include AEIC aircraft emissions (Stettler et al., 2011), POET ethanol (EOH) emissions, Liang bromocarbon emission (Liang et al., 2012), iodocarbon emissions from Ordonez (Sherwen et al., 2016 and references therein), emissions from decaying plants, global ship emissions from ARCTAS, ICOADS, and EMAP, and volcanic eruption and degassing emissions as relevant, and ethane (C2H6) overwritten according to Tzompa-Sosa et al., (2017) for biofuel and anthropogenic sources. We also include the following extensions: SeaFlux, ship emissions (ParaNOx; Vinken et al., 2011), lightning NO_X from global lightning flash distributions (LightNOx; Murray et al., 2012), Dust Entrainment and Deposition (DEAD) scheme allocated to TOMAS15 size bins (Jaeglé et al., 2011), SeaSalt, online MEGAN emissions (Guenther et al., 2012). Biomass burning emissions were from the Global Fire Emissions Database v4 (GFED4) (Van Der Werf et al., 2010) with updated seasonal fire counts following Liu et al., (2019). Trash burning (Wiedinmyer et al. 2014) and anthropogenic fugitive dust (Philip et al., 2017) were only included in the Tropchem runs.

For nested India simulations, the regional emissions inventories for the U.S., Mexico, Canada, Europe, and Africa are not necessary as these regions fall outside the nested domain.

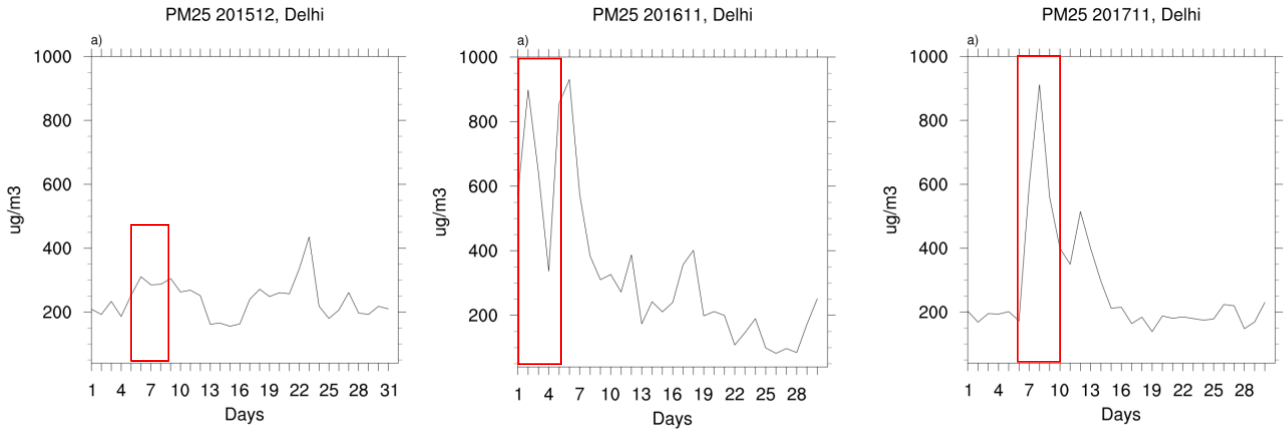

Supplemental Figure 1 Concentrations from the U.S. Embassy in Delhi during December 2015 and November 2016 and 2017. Days in red boxes were chosen to correspond with increases in concentration relative to nearby days.

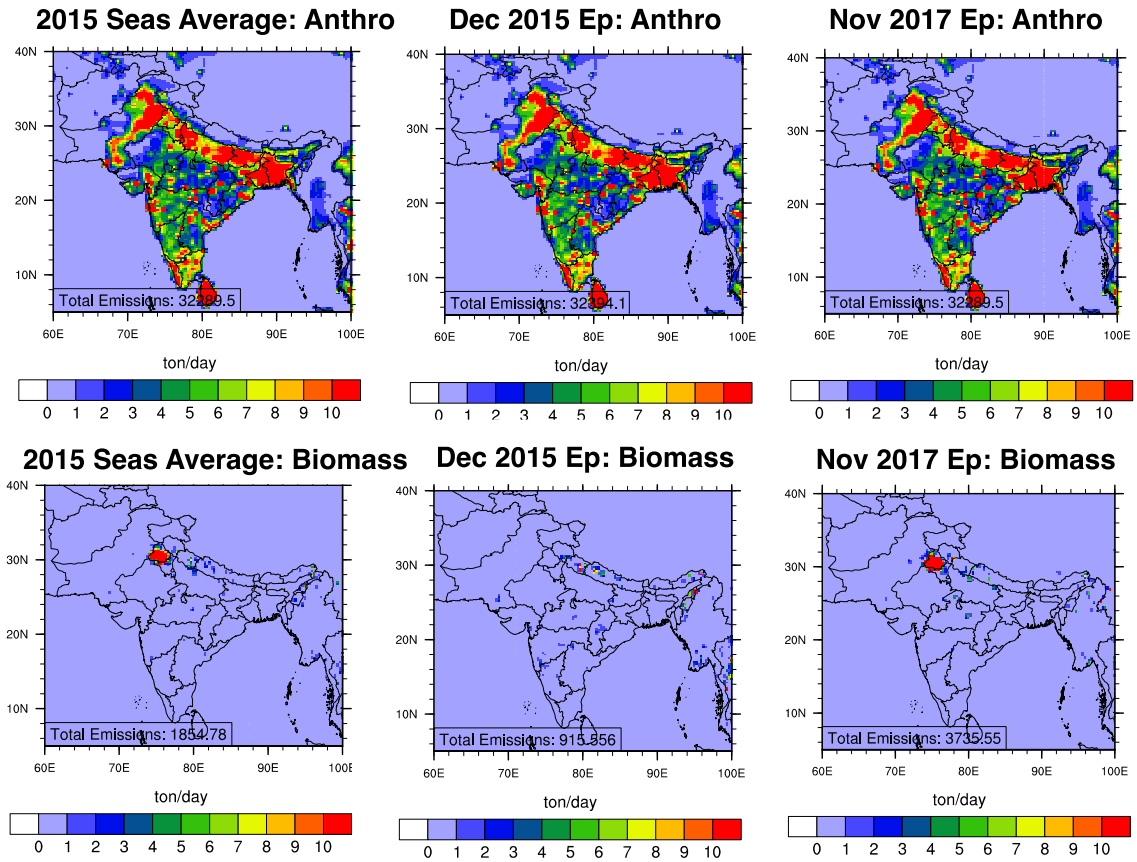

Supplemental Figure 2 Daily average OC emissions for anthropogenic sources (top row) and biomass burning (bottom row) for October to December 2015 (first column), the December 2015 episode (middle column), and the November 2017 episode (right column).

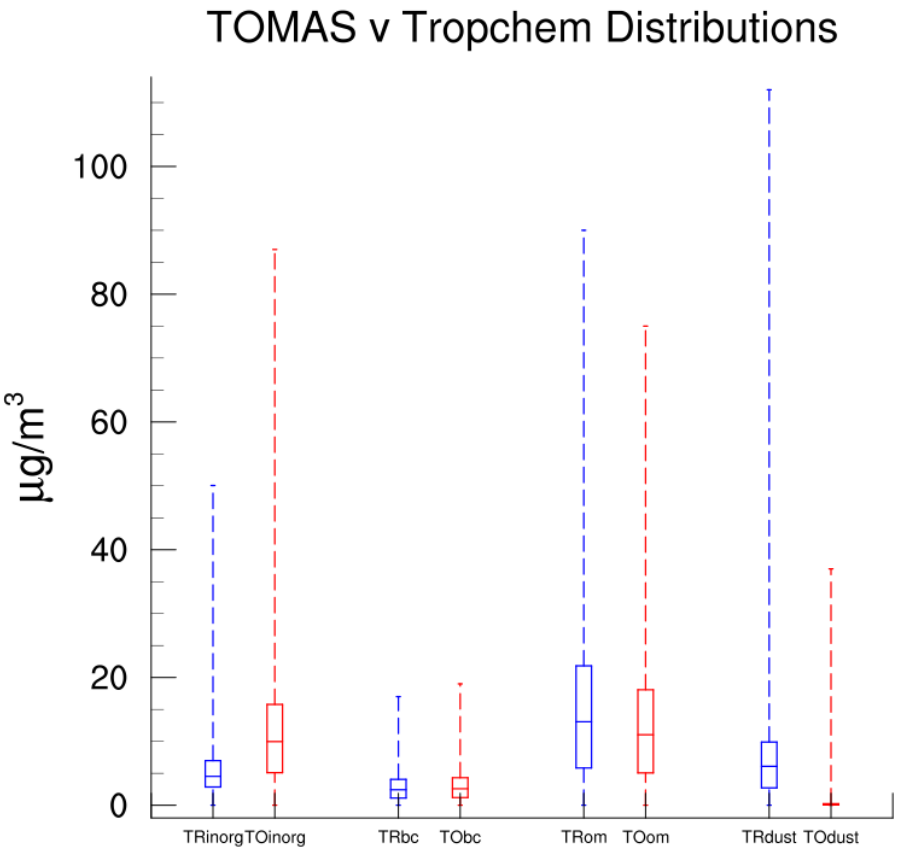

Supplemental Figure 3 Episodic average concentration distribution (minimum, 25th percentile, median, 75th percentile, maximum) for India from the GC-Tropchem (TR) and GC-TOMAS15 (TO) simulations for inorganics (inorg), black carbon (BC), organic matter (OM), and dust. The y-axis is units in µg/m^3. Largest differences occur in dust because the fugitive dust size distribution has not yet been evaluated in TOMAS.

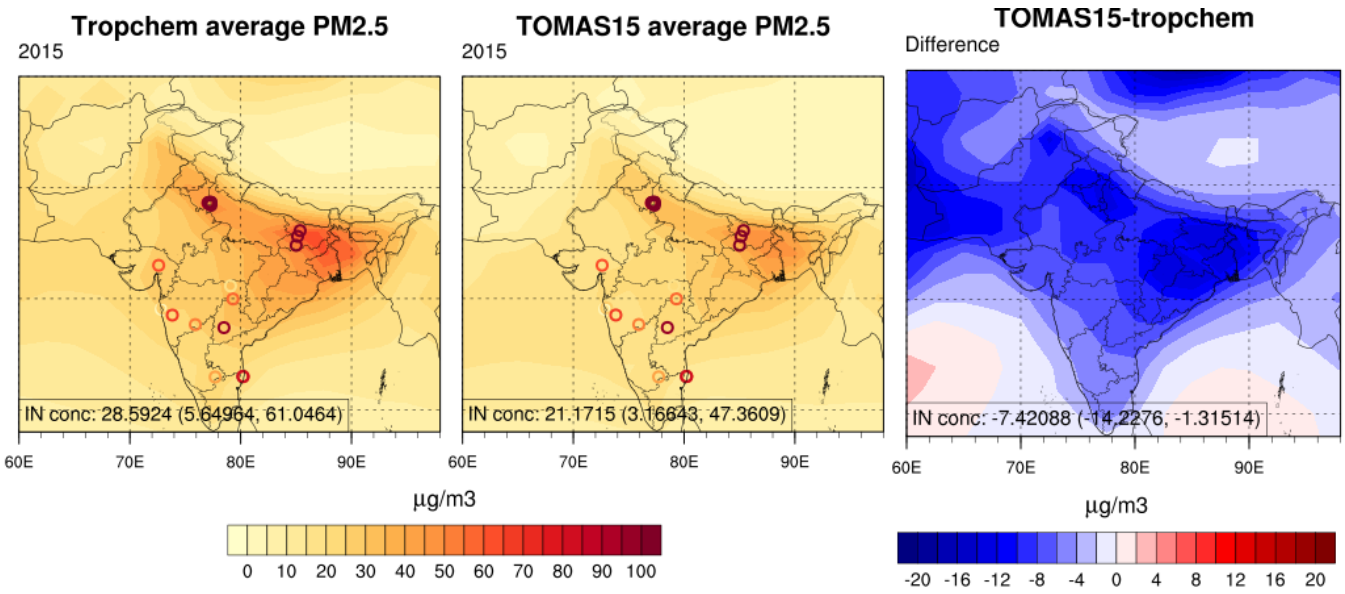

Supplemental Figure 4 Both Tropchem and TOMAS15 global simulations at 2x2.5 horizontal resolution underestimate observed $PM_{2.5}$ concentrations by at least 70 ug/m^3 in the coarse resolution model, yet spatial correlations remain high across the 24 monitor locations ($r^2_{Tropchem}$=0.81 and $r^2_{TOMAS15}$=0.80). The TOMAS15 coarse resolution simulation is systematically lower than Tropchem.

Temporal (e.g. daily average) model evaluation for October-December (Annual) 2015

	Model Average ($\mu g/m^3$)	**Observed Average $\mu g/m^3$)**	**# Points**	**Mean Fractional Bias**	**Normalized Mean Bias**	**Normalized Mean Error**	**r^2**
GC tropchem 2x2.5 (Annual)	48 (36)	139 (98)	1626 (4774)	-76% (-63%)	-66% (-63%)	66% (66%)	0.14 (0.07)
GC TOMAS 2x2.5 (Annual)	59 (38)	139 (98)	1626 (4774)	-60% (-66%)	-58% (-61%)	60% (65%)	0.13 (0.06)
GC tropchem 0.25x0.3125 (Annual)	70 (50)	139 (98)	1626 (4774)	-55% (-45%)	-50% (-49%)	55% (58%)	0.11 (0.06)

Supplemental Table 1 Model evaluation for the October-December daily average across the October to December season with annual comparisons in parenthesis. Correlations are temporal. "Model average" refers to the comparable model average concentration at observation locations.

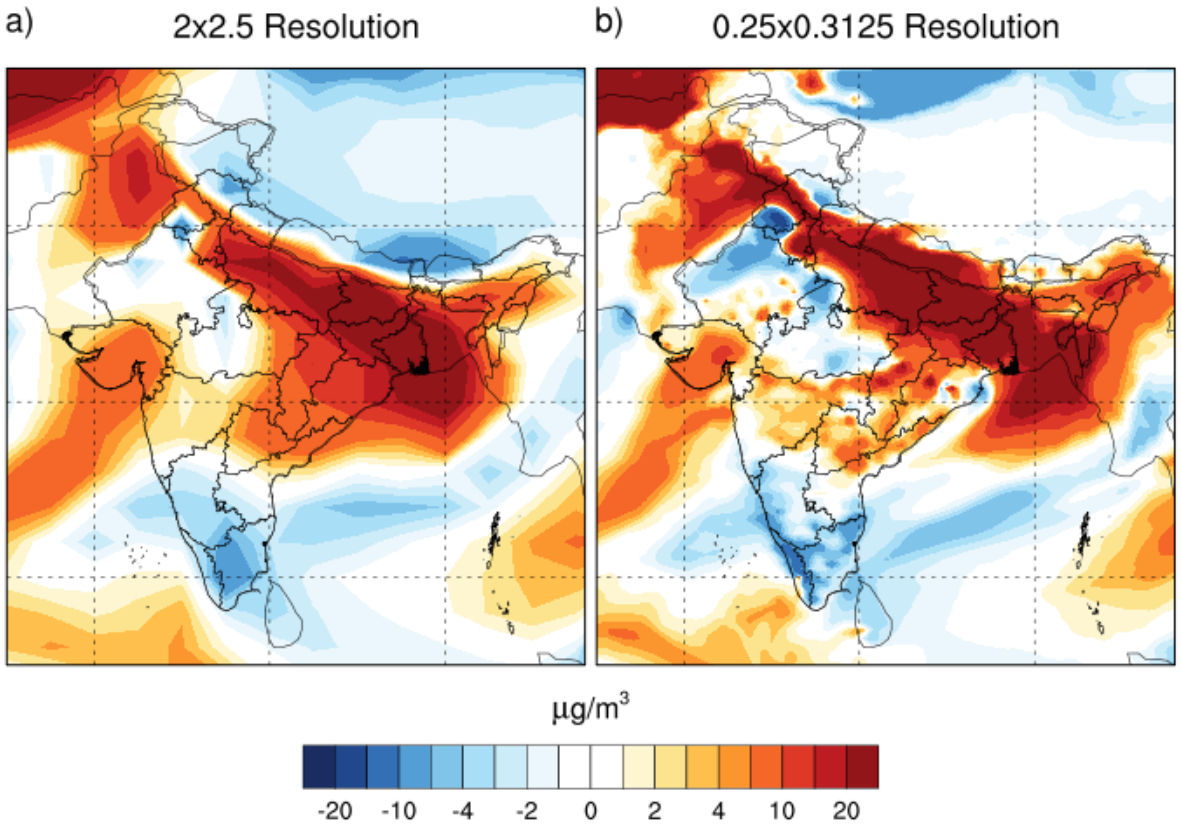

Supplemental Figure 5 Difference plots of the coarse and high resolution simulations using Tropchem for the 2015 pollution episode. Maximum (average) seasonal average concentrations for India are 85.4 $\mu g/m^3$ (32.3 $\mu g/m^3$) for the coarse resolution and 149.4 $\mu g/m^3$ (27.4 $\mu g/m^3$) for the high resolution, and maximum (average) episodic average concentrations are 133.2 $\mu g/m^3$ (38.9 $\mu g/m^3$) for the coarse resolution and 171.7 $\mu g/m^3$ (32.5 $\mu g/m^3$) for the high resolution simulation.

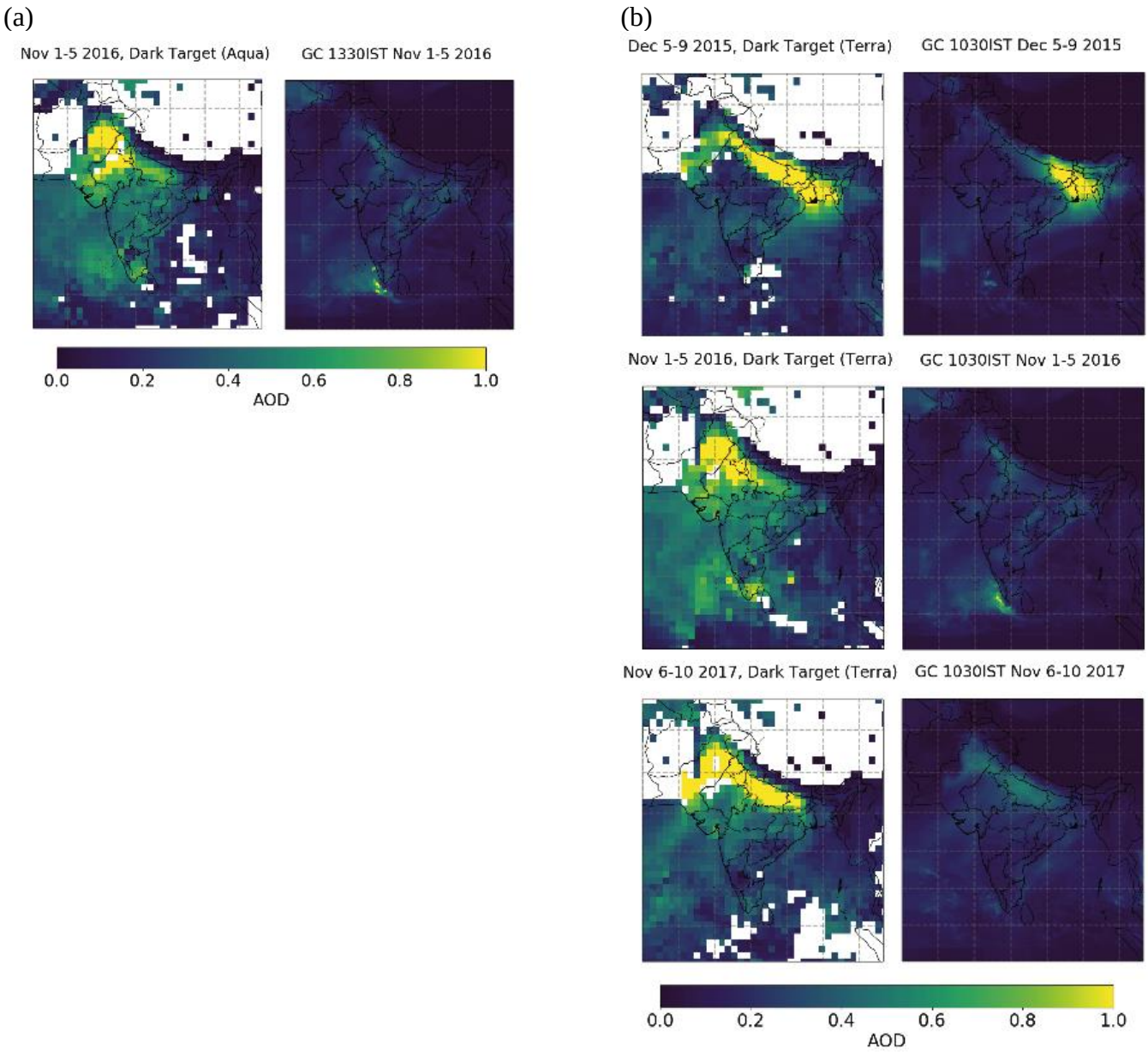

Supplemental Figure 6: MODIS AOD comparison for the (a) November 1-5 2016 pollution episode with MODIS Aqua (see Figure 2 in main text for the other two pollution episodes and (b) for all pollution episodes with MODIS Terra.

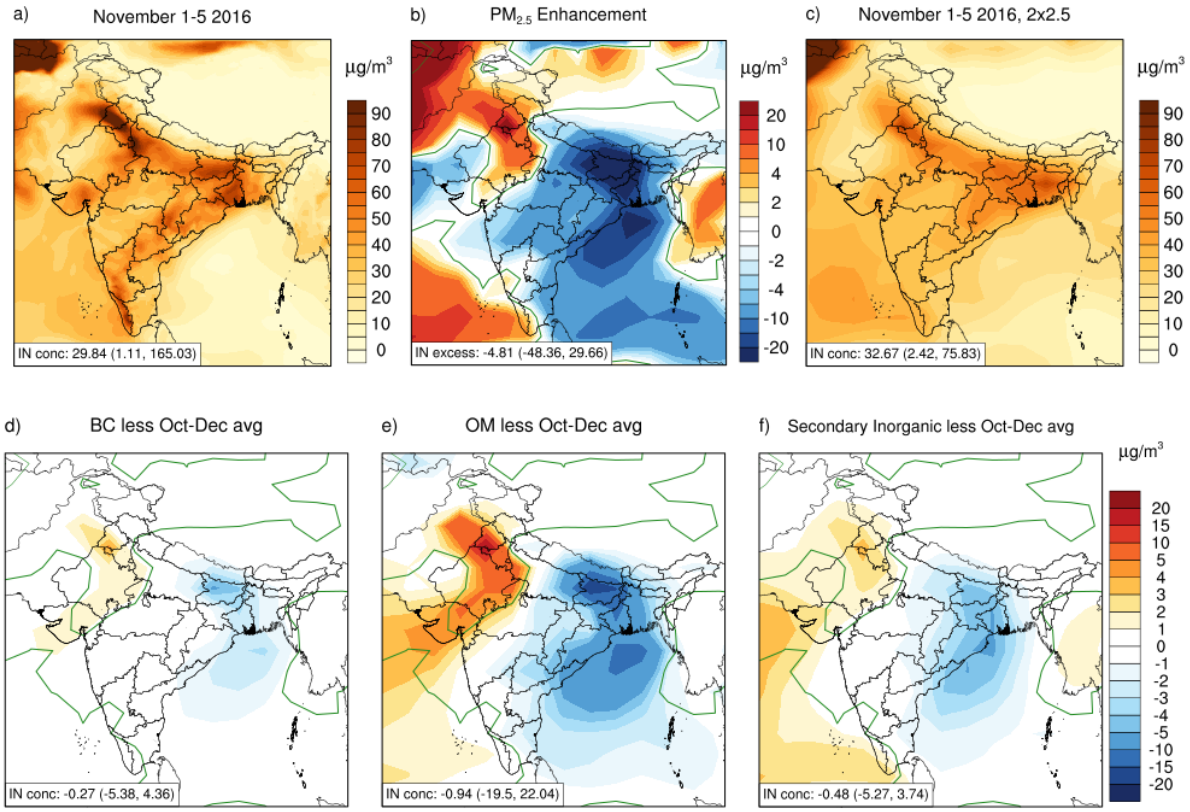

Supplemental Figure 7: Average November 1-5, 2016 episode $PM_{2.5}$ concentration (0.25 x 0.3125 GC-TOMAS15); and concentration enhancements during the episode relative to seasonal average for (all 2 x 2.5) b) $PM_{2.5}$ c) average November 1-5 2016 episode $PM_{2.5}$ concentrations in the 2 x 2x.5 simulation d) black carbon (BC) e) organic matter (OM); f) the sum of inorganic aerosols (sulfate, nitrate, and ammonium). A single contour denoting zero change is superimposed in green.

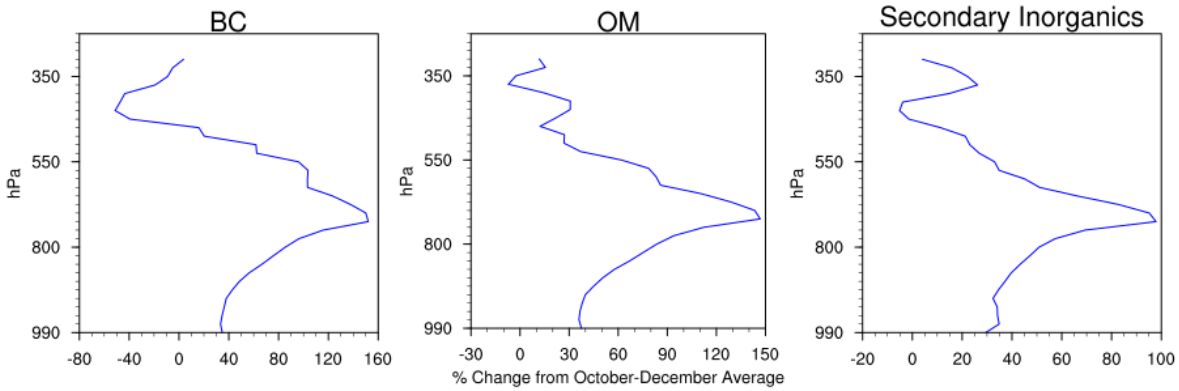

Supplemental Figure 8 Same as Figure 5 except for the November 1-5 2016 episode. Vertical gray bars at 0% indicate no change from seasonal average. Note x-axes ranges indicate smaller changes than for the 2015 and 2017 episodes.

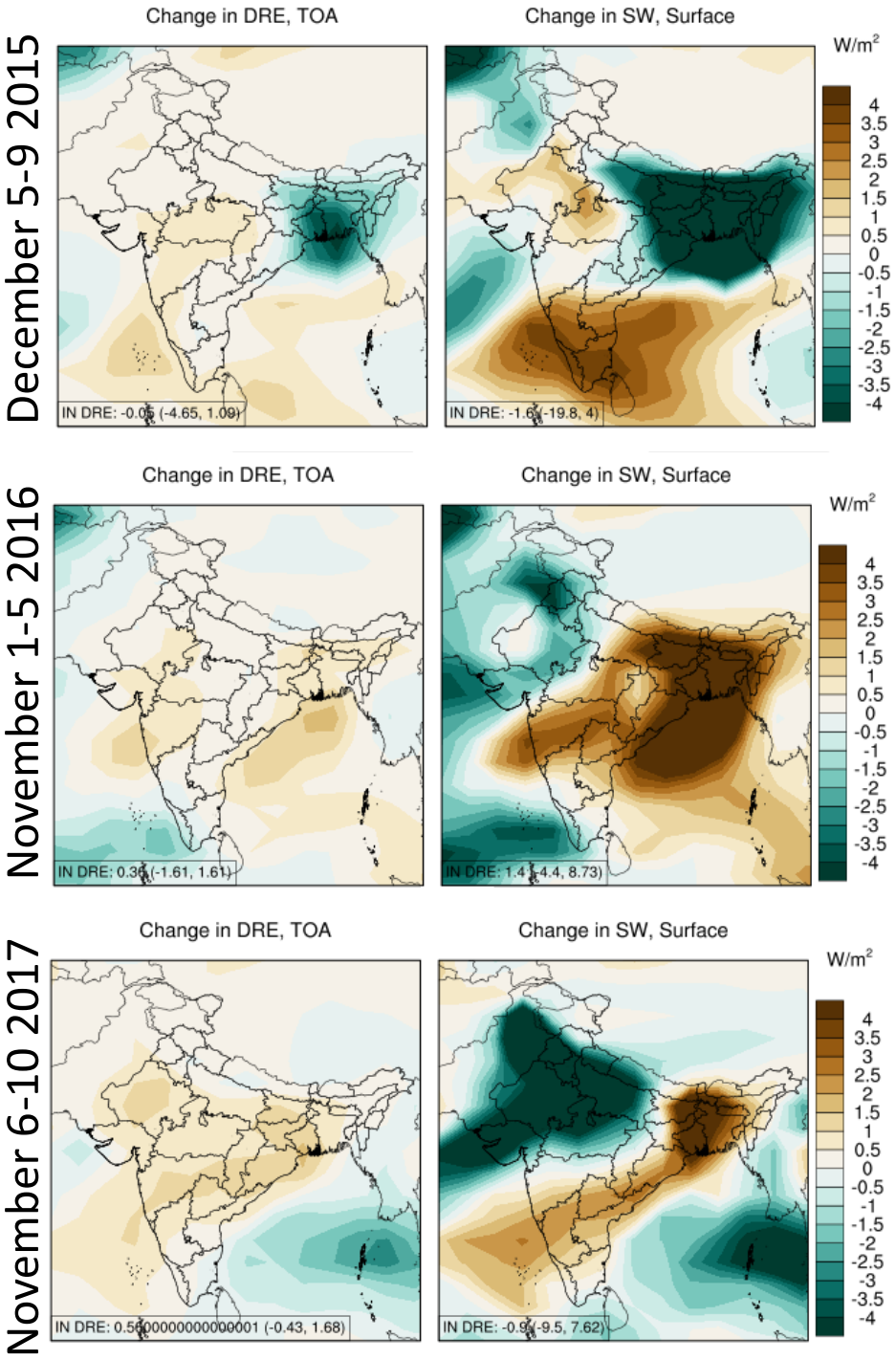

Supplemental Figure 9 RRTMG DRE core-shell between episodes and annual average for (a) 2015 and (b) 2016, and (c) 2017. Negative DRE and SW are indicative of local cooling.

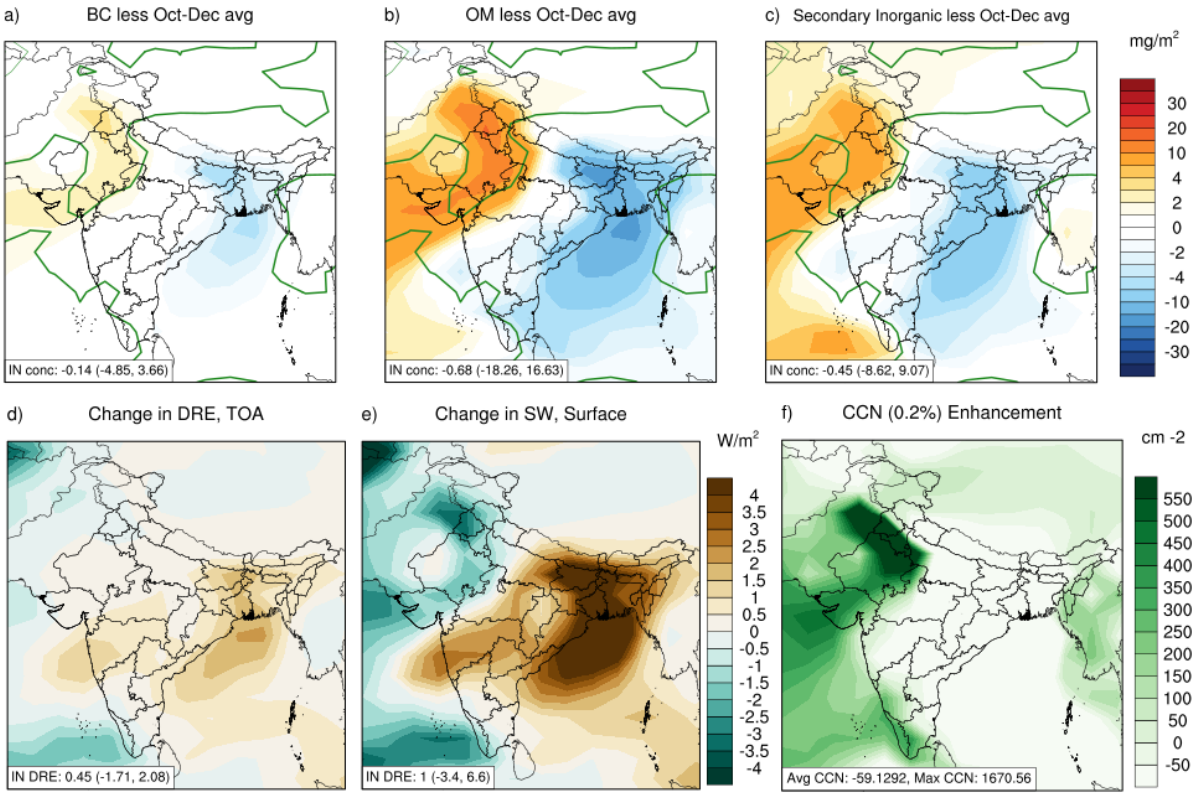

Supplemental Figure 10 Changes in the column burdens of a) black carbon b) organic matter c) secondary inorganics during the November 1-5, 2016 pollution episode from seasonal average (October-December) in the GC-TOMAS15 coarse horizontal resolution (global) simulations (seasonal fields are only available at coarse resolution). Also shown are changes during the episode from the seasonal mean of d) direct radiative effect (DRE) at the top of the atmosphere (TOA); e) net surface shortwave (SW) radiation; f) total column cloud condensation nuclei (0.2% supersaturation). Singular green contour show the line of zero change. Negative DRE and SW are indicative of cooling.

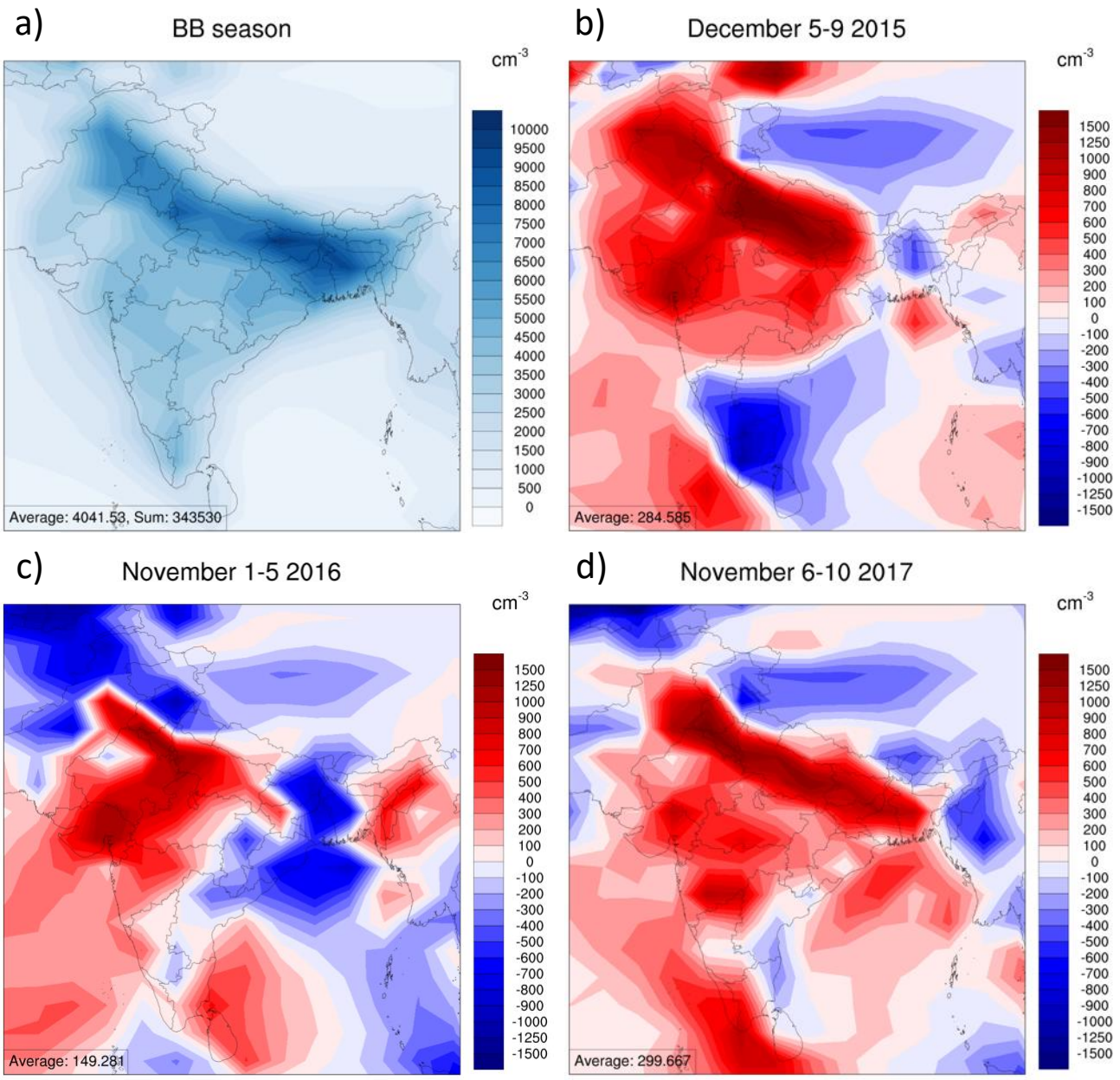

Supplemental Figure 11 Aerosol number concentration for the 2015 biomass burning season (October, November, and December) average, and the change in 2015 episode, 2016 episode, and 2017 episode from respective seasonal average. Distributions during pollution episodes are similar. The total aerosol number concentrations in India increases by approximately 8% (bottom left of each plot), from the biomass burning seasonal average.

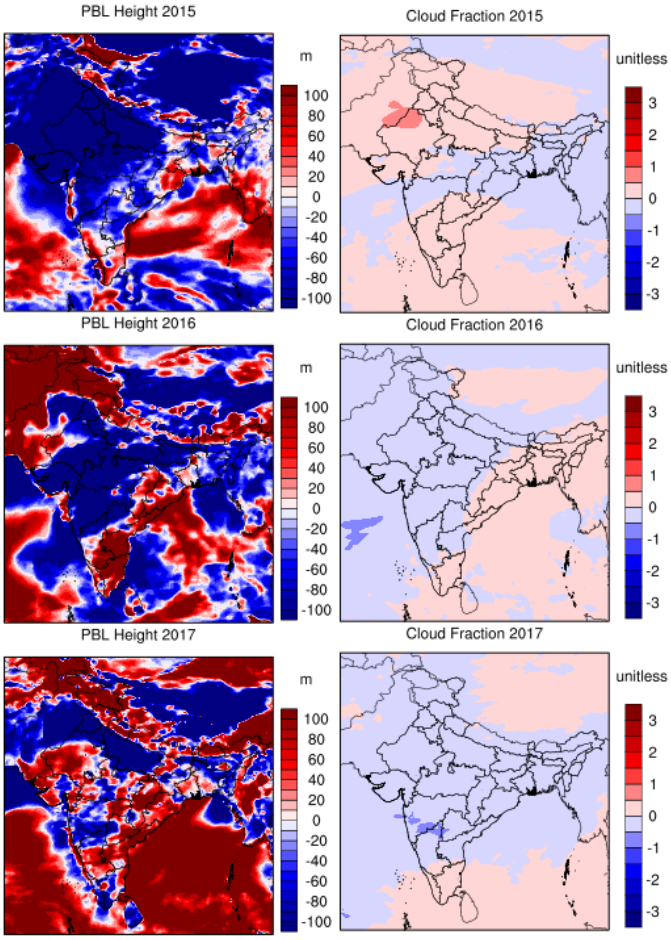

Supplemental Figure 12 Changes in meteorological variables during each episode. Differences between episode and biomass burning seasonal averages (October, November and December) for planetary boundary layer (PBL) height (left column) and cloud fraction (right column).

References

Guenther, A. B., Jiang, X., Heald, C. L., Sakulyanontvittaya, T., Duhl, T., Emmons, L. K., & Wang, X. (2012). The Model of Emissions of Gases and Aerosols from Nature version 2.1 (MEGAN2.1): an extended and updated framework for modeling biogenic emissions. *Geoscientific Model Development*, *5*(6), 1471–1492. https://doi.org/10.5194/gmd-5-1471-2012

Jaeglé, L., Quinn, P. K., Bates, T. S., Alexander, B., & Lin, J.-T. (2011). Global distribution of sea salt aerosols: new constraints from in situ and remote sensing observations. *Atmospheric Chemistry and Physics*, *11*(7), 3137–3157. https://doi.org/10.5194/acp-11-3137-2011

Keller, C. A., Long, M. S., Yantosca, R. M., Da Silva, A. M., Pawson, S., & Jacob, D. J. (2014). HEMCO v1.0: A versatile, ESMF-compliant component for calculating emissions in atmospheric models. *Geoscientific Model Development*, *7*(4), 1409–1417. https://doi.org/10.5194/gmd-7-1409-2014

Liang et al. (2010). Finding the missing stratospheric Br_y: a global modeling study of $CHBr_3$ and CH_2Br_2, Atmos. Chem. Phys., doi:10.5194/acp-10-2269-2010.

Liu, T., Marlier, M., Karambelas, A., Jain, M., Singh, S., Singh, M., et al. (2019). Missing emissions from post-monsoon agricultural fires in northwestern India: regional limitations of MODIS burned area and active fire products. *Environmental Research Communications*, *1*(01), 1007. https://doi.org/10.31223/osf.io/9jvak

Marais, E. and C. Wiedinmyer (2016). *Air quality impact of Diffuse and Inefficient Combustion Emissions in Africa (DICE-Africa)*, Environ. Sci. Technol., 50(19), 10739–10745, doi:10.1021/acs.est.6b02602.

Murray, L. T., Jacob, D. J., Logan, J. A., Hudman, R. C., & Koshak, W. J. (2012). Optimized regional and interannual variability of lightning in a global chemical transport model constrained by LIS/OTD satellite data: IAV OF LIGHTNING CONSTRAINED BY LIS/OTD. *Journal of Geophysical Research: Atmospheres*, *117*(D20). https://doi.org/10.1029/2012JD017934

Philip, S., Martin, R. V., Snider, G., Weagle, C. L., van Donkelaar, A., Brauer, M., et al. (2017). Anthropogenic fugitive, combustion, and industrial dust is significant, underrepresented fine particulate matter source in global atmospheric models. *Environmental Research Letters*, *044018*. https://doi.org/10.1088/1748-9326/aa65a4

Sherwen, T., Schmidt, J. A., Evans, M. J., Carpenter, L. J., Großmann, K., Eastham, S. D., et al. (2016). Global impacts of tropospheric halogens (Cl, Br, I) on oxidants and composition in GEOS-Chem. *Atmospheric Chemistry and Physics*, *16*(18), 12239–12271. https://doi.org/10.5194/acp-16-12239-2016

Stettler, M. E. J., Eastham, S., & Barrett, S. R. H. (2011). Air quality and public health impacts of UK airports. Part I: Emissions. *Atmospheric Environment*, *45*(31), 5415–5424. https://doi.org/10.1016/j.atmosenv.2011.07.012

Tzompa-Sosa, Z. A., Mahieu, E., Franco, B., Keller, C. A., Turner, A. J., Helmig, D., et al. (2017). Revisiting global fossil fuel and biofuel emissions of ethane. *Journal of Geophysical Research: Atmospheres*, *122*(4), 2493–2512. https://doi.org/10.1002/2016JD025767

Van Der Werf, G. R., Randerson, J. T., Giglio, L., Collatz, G. J., Mu, M., Kasibhatla, P. S., et al. (2010). Global fire emissions and the contribution of deforestation, savanna, forest, agricultural, and peat fires (1997-2009). *Atmospheric Chemistry and Physics*, *10*(23), 11707–11735. https://doi.org/10.5194/acp-10-11707-2010

Vinken, G. C. M., Boersma, K. F., Jacob, D. J., & Meijer, E. W. (2011). Accounting for non-linear chemistry of ship plumes in the GEOS-Chem global chemistry transport model. *Atmospheric Chemistry and Physics*, *11*(22), 11707–11722. https://doi.org/10.5194/acp-11-11707-2011